10 Tandem Configuration in Hover

In this chapter, a hovering tandem configuration has been studied using a time-resolved PIV system (see section 3.7.2). For these measurements shadows and reflections were minimal such that a complete control-volume analysis could be performed in order to obtain normal (C_n) and thrust forces (C_t) acting in the vertical and horizontal directions, respectively. These forces are non-dimensionalized using the maximum plunge velocity ($\dot{h}_{max}$). Using these time-resolved forces, tandem cases with similar performance to the single airfoil have been examined. Particular focus is placed on power consumption and specific vortex interactions unique to the tandem configuration.

10.1 Parameter Space

The pitching and plunging movement of the fore- (F) and hindfoils (H), in this case flat plates, can be described through Eq. (10.1)-(10.4), where the hindfoil leads the forefoil with a phase angle ψ:

$$h_F = h_o \cos(2\pi f t) \tag{10.1}$$

$$\alpha_F = \alpha_o + \alpha_1 \cos(2\pi f t + \phi) \tag{10.2}$$

$$h_H = h_o \cos(2\pi f t + \psi) \tag{10.3}$$

$$\alpha_H = \alpha_o + \alpha_1 \cos(2\pi f t + \phi + \psi) \tag{10.4}$$

For both profiles, pitching lead plunging by a phase angle of $\phi = 90°$.

The dimensionless plunge amplitude for all cases, based on the quarter-chord position ($c/4$), was maintained at $h = \pm 0.5\,c$, as described in the previous chapter for cruise conditions. The rotation points for both fore- and hindfoil were fixed at the quarter-chord position and the airfoil spacing was again set at $S = 2\,c$ between the airfoil quarter-chord positions. Both profiles were oscillated symmetrically about $\alpha_o = 0°$, whereas the pitch amplitude was set to the rig's maximum of $\alpha_1 = 30°$. Lehmann (2009) used $\alpha_1 = 45°$ in his study, however, the vortex formation is expected to be quite similar since full separation was maintained throughout the cycle. Finally, the dynamic motions were set to a frequency of $f = 1$Hz, corresponding to a maximum plunge velocity of $\dot{h}_{max} = 0.38$m/s. The Reynolds number based on this plunge velocity was approximately Re=3000, which corresponded to turbulent transition in the leading- and trailing-edge shear layers. The airfoil phasing (ψ) was varied in 45° increments, i.e. from $\psi = 0°$ through to $\psi = 315°$. For each phasing, an experimental run with seven cycles was performed approximately 15-20 times, with the exception of $\psi = 180°$, 225°, 270° and 315°, where only three experimental runs were performed for each phasing.

10.2 Time-Resolved Forces

In the following section, the time-dependent behavior of the dimensionless aerodynamic forces are presented. First the time-resolved forces for two exemplary experimental runs are shown. This comparison is used to provide an overview of the global force variation. Afterwards the fourth cycle is extracted and presented since it has been deemed most representative of dragonfly hover flight.

10.2.1 Complete Run

When examining the forces in Fig. 10.1 and Fig. 10.2, one notices that the first two to three cycles are non-periodic and therefore have been discarded in the later discussion. One may note that for both reference case and $\psi = 90°$ that the peak-to-peak value of C_t decreases in time. This is explained by the limitations of the experimental setup. The experimental chamber was $x/c = 4.75$ long and therefore after several cycles the induced wake was gradually influenced by the back wall of the hover chamber.

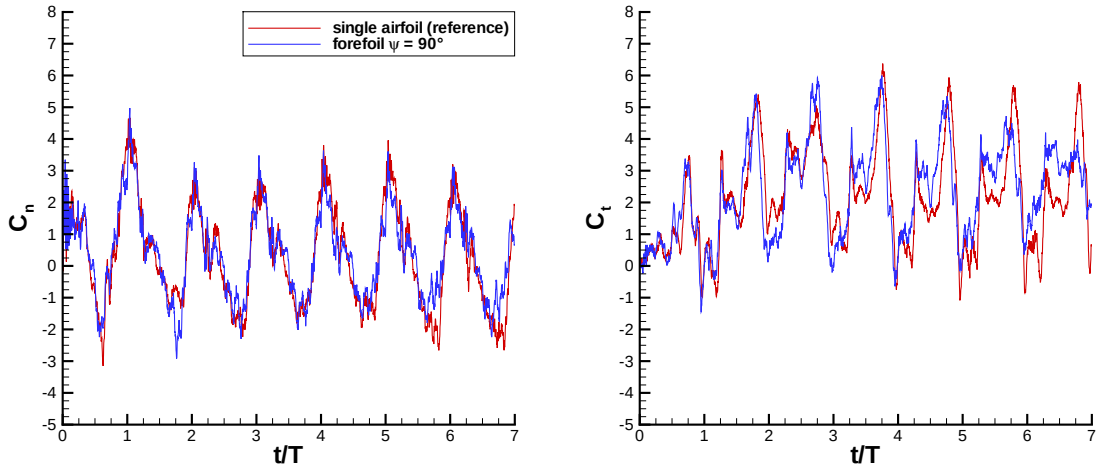

(a) normal (b) thrust

Figure 10.1: Ensemble-averaged normal force (a) and thrust force (b) for the forefoil during an experimental run.

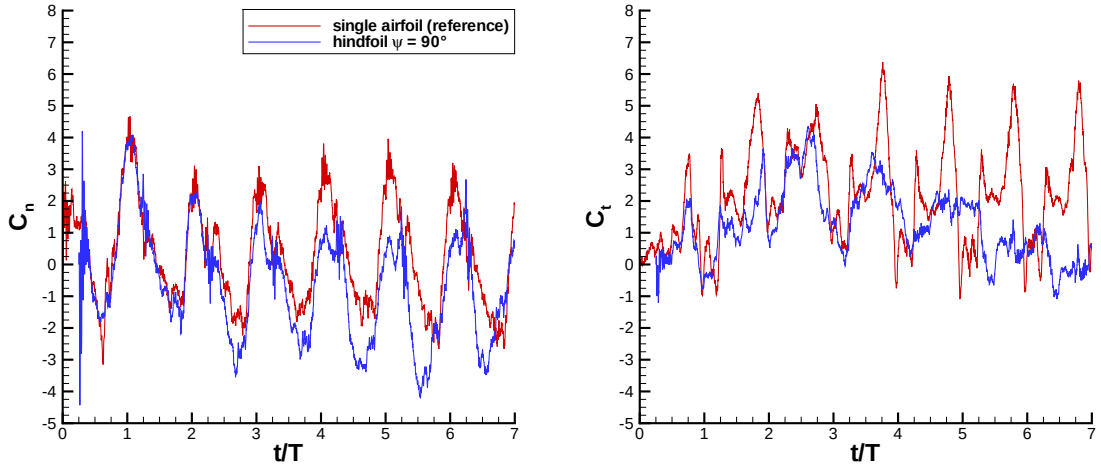

(a) normal (b) thrust

Figure 10.2: Ensemble-averaged normal force (a) and thrust force (b) for the hindfoil during an experimental run; note plots of $\psi = 90°$ for the hindfoil are shifted in time in a manner that the hindfoil is always at TDC at t/T = 0.

Because the fourth cycle shows the highest amplitude and a representative force variation over the cycle (found for all experimental runs), it has been used throughout this study since it is least affected by both initial and boundary conditions. Between 15-20 experimental runs were performed for all cases such that ensembles of the fourth cycle could be used for a proper statistical analysis of the flow.

10.2.2 Representative Cycle

As demonstrated in the previous section the fourth cycle is the most representative cycle of the experiment. Fig. 10.3 and Fig. 10.4 show the fourth cycle of the $\psi = 90°$ case with its first standard deviation of the cycle-to-cycle variations plotted at 25-timestep intervals. The single-airfoil results are also presented, but without error bars to maintain clarity. One may notice in both figures that the standard deviation tends to be higher on the hindfoil, especially for the normal force. Overall the standard deviation fluctuates between 0.5 and 1.5 and can be explained by the inherent stochastic vortex-body interaction associated with such fully-separated flows. Nevertheless the temporal variation of C_n and C_t is repeatable when examining one experimental run to the next.

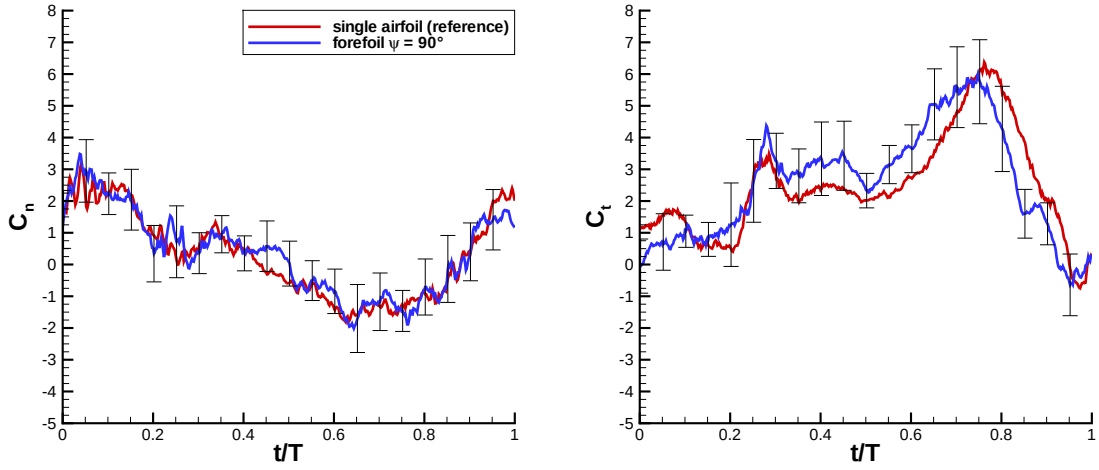

(a) normal (b) thrust

Figure 10.3: Ensemble-averaged normal force (a) and thrust force (b) for forefoil during representative cycle.

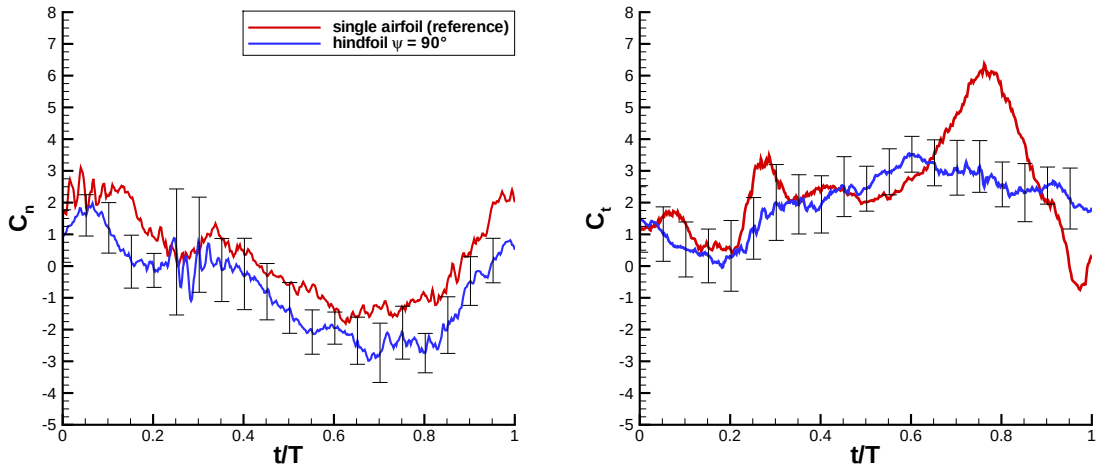

(a) normal (b) thrust

Figure 10.4: Ensemble-averaged normal force (a) and thrust force (b) for hindfoil during representative cycle; note plots of $\psi = 90°$ for the hindfoil are shifted in time in a manner that the hindfoil is always at TDC at t/T = 0.

10.3 Mean Forces

10.3.1 Combined

In Fig. 10.5 the dependency of the combined (fore- and hindfoil) mean normal and thrust coefficients versus phase angle (ψ) are presented. The normal force of the reference case shows a small positive value. This can be explained by the asymmetry of the initial condition (the airfoil was always started at one end of the stroke). When examining the combined normal forces, the dependency on phase angle is found to be weak. For $\psi = 0°$, $\psi = 45°$ and $\psi = 180°$ the normal force is negligibly small. Only at $\psi = 135°$ is the absolute value of the normal force higher than the reference case. The tandem cases show in this sense a better performance than the reference case since lateral forces in hover should ideally be minimized.

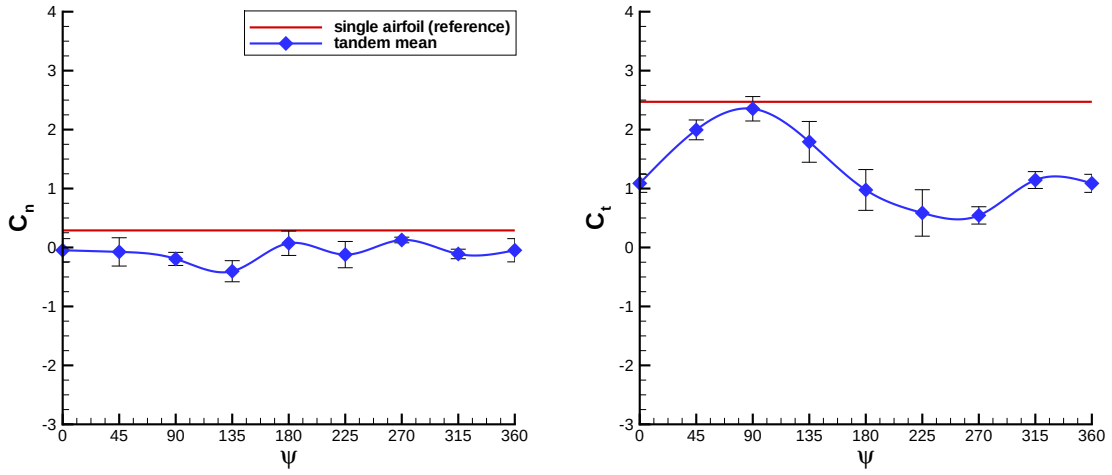

(a) normal (b) thrust

Figure 10.5: Influence of the phase angle (ψ) on combined/averaged (fore- and hindfoil) normal force (a) and thrust force (b).

The combined thrust varies sinusoidally with the phase angle. The maximum thrust is observed at $\psi = 90°$. The lowest thrust values are measured at $\psi = 225°$ and $\psi = 270°$, which agree with the measurements made by Lehmann (2009). Although the reference case's thrust is higher than the mean thrust forces for all phase angles, certain individual cycles for $\psi = 90°$ show higher values. Also of interest, the standard deviation of the $\psi = 135°$ and $\psi = 180°$ cases are significantly higher than for the other phases. This is due to an unstable behavior of the vortex trajectories, again a function of the stochastic nature of the flow.

10.3.2 Forefoil

Examining the forefoil's normal and thrust forces over different phase angles, one finds similar values to the single-airfoil case. Especially the normal forces with low phase angles ($0° \leq \psi \leq 135°$) match the reference case almost perfectly. The only phase to show a large deviation in the normal force is $\psi = 135°$. The thrust forces for small phase angles ($0° \leq \psi \leq 90°$) match the reference case also very closely. The higher phase angles (again with the exception of $\psi = 315°$) produce even larger thrust. As with the normal forces, the thrust of the forefoil shows little variation with the different phase angles.

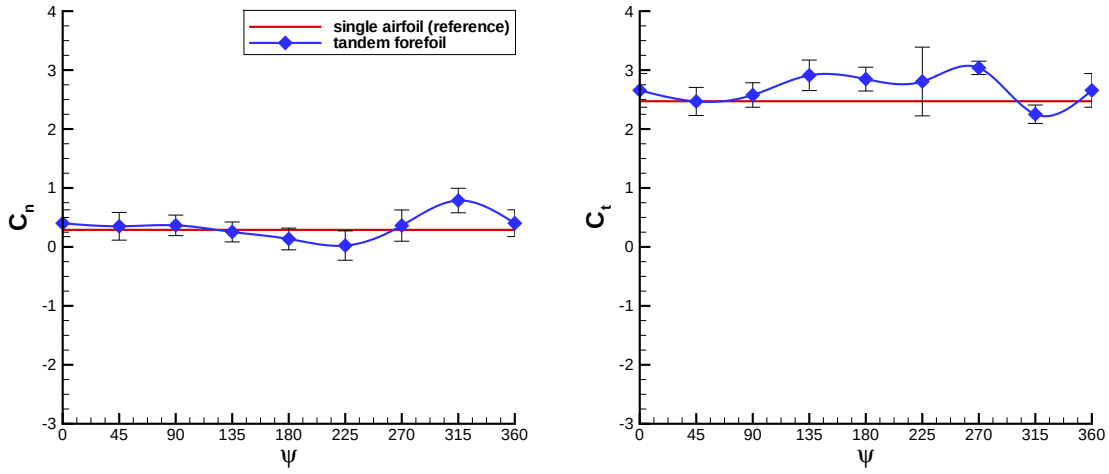

(a) normal (b) thrust

Figure 10.6: Influence of the phase angle (ψ) on mean normal force (a) and thrust force (b) for forefoil.

10.3.3 Hindfoil

While the forefoil's normal and thrust forces share similar values with the reference case and thus very similar vortex development, the hindfoil's forces vary drastically due to the strong vortical inflow. Hence the force variation with phase angle for the hindfoil varies drastically. This strong variation with phasing is presented in Fig. 10.7.

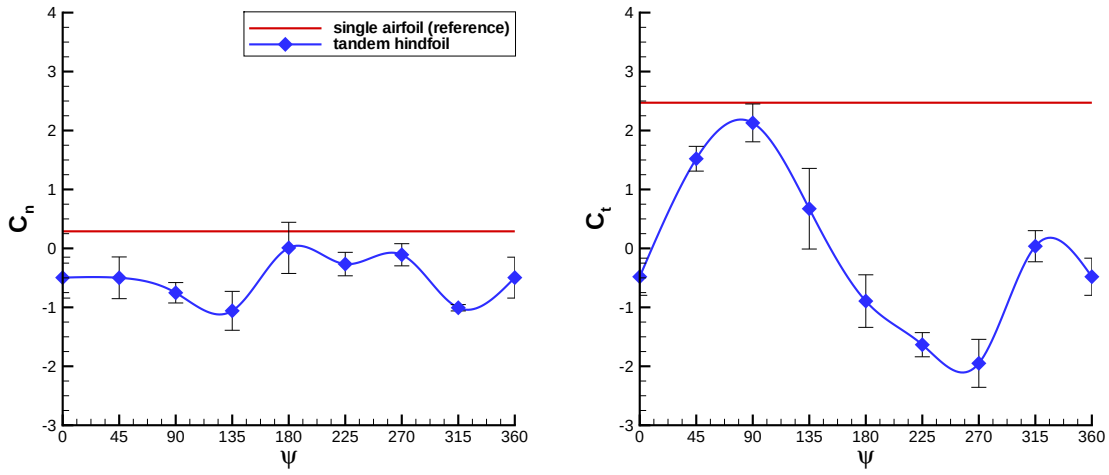

(a) normal (b) thrust

Figure 10.7: Influence of the phase angle (ψ) on mean normal force (a) and thrust force (b) for hindfoil.

The normal force shows two different levels. The first plateau is situated at $C_n = -0.5$ and appears for $0° \leq \psi \leq 90°$. The second plateau is situated at $C_n = 0$ and appears for $180° \leq \psi \leq 270°$. Between these two levels the normal force decreases to $C_n = -1$ at phase angles of $\psi = 135°$ and $\psi = 315°$.

The thrust force shows a sinusoidal dependency to phase angle. While the forefoil produces thrust at all phase angles, the hindfoil does so only for $45° \leq \psi \leq 135°$. For other phase angles the force is negative, i.e. drag is produced. Moreover the standard deviations for the $\psi = 135°$ and $\psi = 180°$ cases are clearly larger than for the other cases. The transient behavior of the thrust force as well as the higher standard deviation of the particular phase angles depend on varying trajectories of the forefoil's trailing-edge vortex (see section 10.5). Thus it is clear that the difference between the reference case and the combined forces depends predominantly on the hindfoil's capacity to produce thrust in the forefoil's oncoming wake.

10.4 Power Consumption

In the previous sections it has been shown that a tandem configuration provides no net advantage in terms of maximum force compared to two independently-moving single airfoils. To investigate the possibility of a reduction in energy consumption, the necessary power to overcome the aerodynamic forces due to the airfoil motion has been calculated. It should be noted here that the power consumption associated with the pitch movement has been neglected since it accounts for less than 10% of the total power in the most extreme case.

10.4.1 Time-Resolved Power

The power consumption of the forefoil for the various cases is to a large extent similar. In particular the power consumption for the $\psi = 90°$ case is almost identical to that of the reference case over the entire cycle. In the first half-cycle the $\psi = 0°$ case has the same structure as the $\psi = 90°$ and the reference cases, while the $\psi = 180°$ case shows the largest deviation. In addition the $\psi = 180°$ case reaches its maximum in the first half-cycle at $t/T = 0.25$ while all other cases reach their maximum during the first half-cycle at approximately $t/T = 0.125$. In the second half-cycle only the $\psi = 0°$ case shows significant deviation to the reference case. Thereby the forefoil consumes significant less power than the reference case between $t/T = 0.75$ and $t/T = 1$. Interesting is that all cases are able to recover energy between $t/T = 0.85$ and $t/T = 1$.

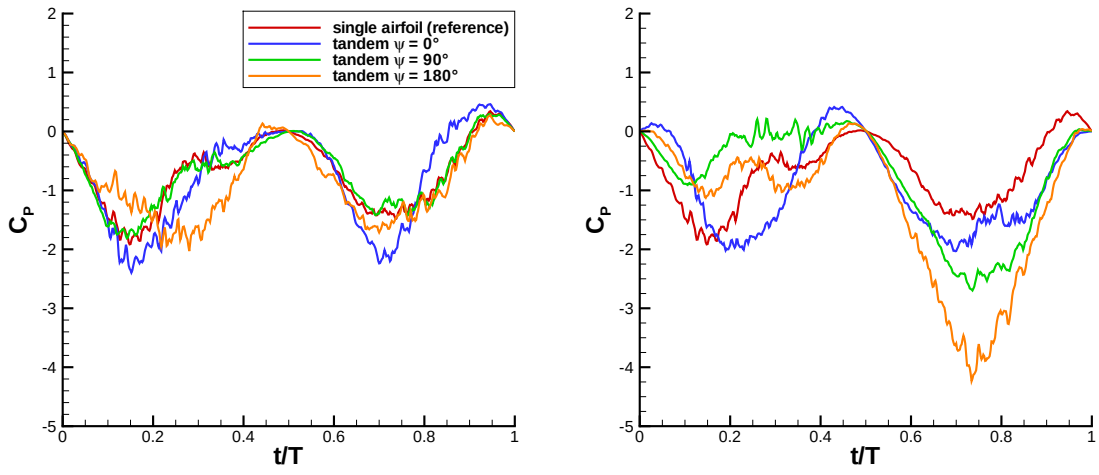

(a) forefoil (b) hindfoil

Figure 10.8: Nondimensional time-resolved power for the fourth cycle; note plots for the hindfoil are shifted in time in a manner that the hindfoil is always at TDC at t/T = 0.

The plot for the hindfoil shows much stronger deviations between the various cases. At the beginning of the first half-cycle all tandem cases consume less power than the reference case. Furthermore the $\psi = 0°$ case consumes less power than the reference case during the entire first half-cycle. In the period between $t/T = 0.25$ and $t/T = 0.5$ the power consumption of the $\psi = 0°$ case is almost zero. As well the $\psi = 180°$ case consumes less power than the reference case during most of the first half-cycle. However, during the second half-cycle the tandem cases show no advantage compared to the reference case.

When comparing the power consumption of the hindfoil overall, one may recognize that no clear advantage can be observed for the various cases since the advantages found in the first half-stroke are always canceled out by the poorer performace in the second half of the cycle. However, for the $\psi = 90°$ case, the reduction of the downstroke actuator size (or muscle for a biological system) due to the reduced power requirement between $t/T = 0.25$ and $t/T = 0.5$ would be possible. In fact, from a physiological standpoint, dragonflies are known to have drastically different sized muscles for the two half strokes, thus perhaps explaining the necessity of wing phasing.

10.4.2 Mean Power

Since the analysis of the time-resolved power did not immediately identify a favorable tandem case, the mean power consumption for the fourth cycle was calculated and is presented in Fig. 10.9. As one could expect from the forefoil's time-resolved power distribution in Fig. 10.8(a), only phase angles around $\psi = 90°$ consume as little energy overall as the reference case, while all other tandem cases consume significantly more. For the hindfoil, only the $\psi = 270°$ and $\psi = 315°$ cases consume less energy than the reference case, however, thrust is poor for these phasings. When considering the mean consumption no tandem case clearly exceeds the performance of the reference case. However, as mentioned above the $\psi = 90°$ cases uses similar levels of power, but distributed at different points over the cycle, which potentially might be of vital importance in terms of actuation for MAV systems.

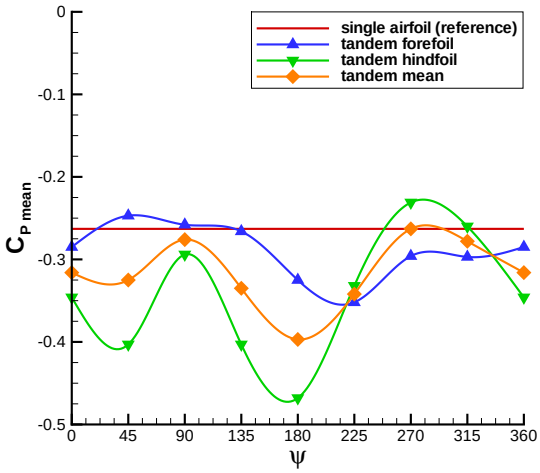

Figure 10.9: Nondimensional mean power as function of phase angle (ψ).

10.5 Vortex Interaction

Since the $\psi = 90°$ case is the only case producing a similar level of thrust when compared to the reference case, as shown above in Fig. 10.5(b), its flow field has been examined in detail. The comparison between the forefoil and the reference case flow fields show strong similarities. Furthermore their time-resolved forces are nearly identical, as presented in Fig. 10.1. However, the hindfoil force development, particularly for the thrust component, shows distinct differences compared to the reference case, as depicted in Fig. 10.4. These differences can be explained by examining the associated velocity and vortical fields in Figs. 10.11 - 10.13. Note every fifth velocity vector is plotted in the x-direction for sake of clarity.

10.5.1 Effects on Thrust Force

Examining the thrust-producing mechanisms of the single airfoil, one finds flow structures which can be associated with each of the two peaks ($t/T = 0.25$ and $t/T = 0.75$) shown in Fig. 10.4(b). It emerges that the vortical structures relating to these peaks are pairs of vortices with opposite sign establishing a reverse *von Kármán* street behind the foil. The first peak in the force diagram at $t/T = 0.25$ (for flow field see Fig. 10.11) arises just before the downstroke TEV begins to break-off the hindfoil surface. Examining the subsequent time steps, one finds that the strength of the TEV remains fairly constant from $t/T = 0.375$ until $t/T = 0.625$, as identified in Fig. 10.10. This results in a constant thrust force in this time period.

Simultaneously the upstroke TEV grows rapidly because of the strong influence of the downstroke TEV on the developing shear layer, see Fig. 10.12 and Fig. 10.13 time steps $t/T = 0.625$ to $t/T = 0.875$. With the creation of the upstroke TEV, the second pair of counter-rotating vortices is formed during the upstroke establishing a strong jet, which results in the second, more substantial thrust peak as seen at $t/T = 0.75$ in Fig. 10.4(b). Due to the mutually-induced velocity, the vortex pair convects away from trailing edge and therefore thrust decreases rapidly.

The comparison of the flow field and thrust force development of the single airfoil with the tandem configuration shows several distinct differences. For one, the forefoil TEV strengthens the shear layer at the hindfoil leading edge as it passes by. This interaction encourages an earlier formation of the hindfoil LEV, which can be clearly seen at $t/T = 0.25$ in Fig. 10.11. This mechanism has been previous identified by Maybury and Lehmann (2004). This earlier formation of the LEV in turn shifts the hindfoil TEV further backwards. Finally at $t/T = 0.625$, the thrust force on the hindfoil remains fairly constant, in contrast to the single-airfoil case where the more compact spacing of the TEV is found to be responsible for generating the stronger jet and therefore the higher thrust peak. Despite the lack of these thrust peaks, the tandem configuration allows for a constant production of thrust over the cycle, which might be of importance during predation, as discussed by Alexander (1984).

In the meantime, the upstroke LEV over the hindfoil is again developed earlier due to the interaction of the shed TEV from the forefoil, see time step $t/T = 0.625$ in Fig. 10.12. This faster development of the LEV again influences the relative positioning of the upstroke TEV through induction, pulling the developing TEV further forward in comparison to the single airfoil. This stronger interaction between the hindfoil LEV and TEV is responsible for the quick elimination of the LEV by time step $t/T = 1$. For the single-airfoil case, a strong LEV is present at this timestep and thus hinders the production of a downstroke LEV on the following halfstroke.

10.5.2 Effects on Normal Force

In comparison to the single airfoil, the normal force on the hindfoil shows a similar trend but is slightly offset towards zero. The establishment of thrust on the forefoil results in the passing of strong vortex pairs past the hindfoil, as can be seen at $0 \leq t/T \leq 0.25$ in Fig. 10.11 as well as at $0.75 \leq t/T \leq 1$ in Fig. 10.13. In both of these periods the jet is directed beneath the hindfoil. The high flow velocities induced by this jet result in suction, which acts to cancel out the normal forces created by the hindfoil LEV at $t/T = 0.25$. Similarly the influence on the positioning of the TEV, as discussed in the above section, influences the generation of these normal forces as well. This cancelation of the normal force during the first halfstroke reduces the power consumption significantly whereby the increased normal force on the second halfstroke naturally increases power consumption, as found in Fig. 10.8(b).

10.5.3 Behavior of TEV

When examining the behavior of the downstroke TEV more closely in Fig. 10.10, one can observe in the first half of the cycle that the vertical TEV positions are nearly identical but that the TEV circulation in the tandem arrangement is stronger. Conversely in the second half of the cycle, the TEV circulation is similar but the spacing between the TEV and the single airfoil decreases rapidly whereas for the tandem case the TEV convects out in a horizonal path. During the first halfstroke, the increased TEV circulation assists in the reduction of the normal force in the tandem arrangement, see Fig. 10.8(b). For the second halfstroke, however, the larger spacing between TEV and hindfoil in the tandem arrangement reduces the strength of the jet, as discussed in section 10.5.1. Again, the main influence on the strength and positioning of this TEV is the formation of the hindfoil LEV, which is found to be drastically influenced by the interaction with the forefoil.

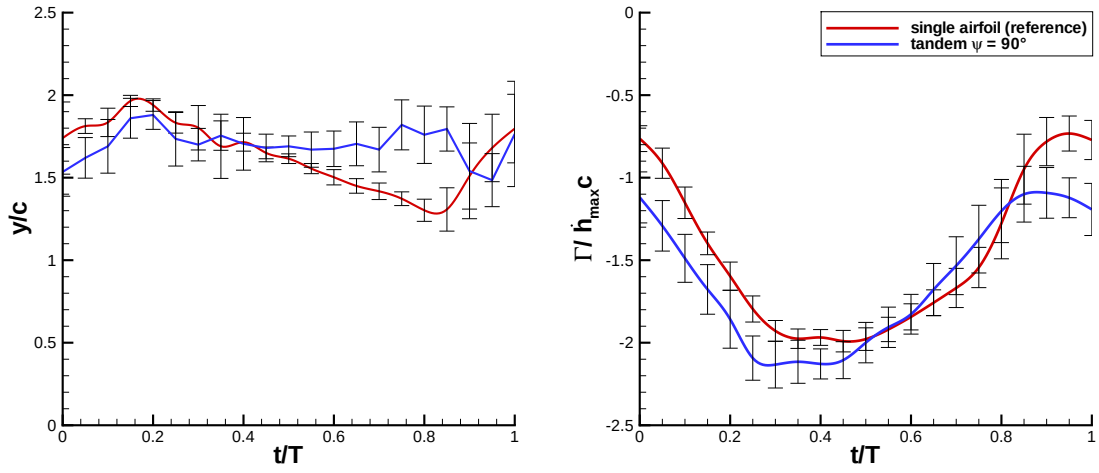

(a) trajectory (b) circulation

Figure 10.10: Trajectories and nondimensional circulation of downstroke TEV from single airfoil and tandem configuration with $\psi = 90°$.

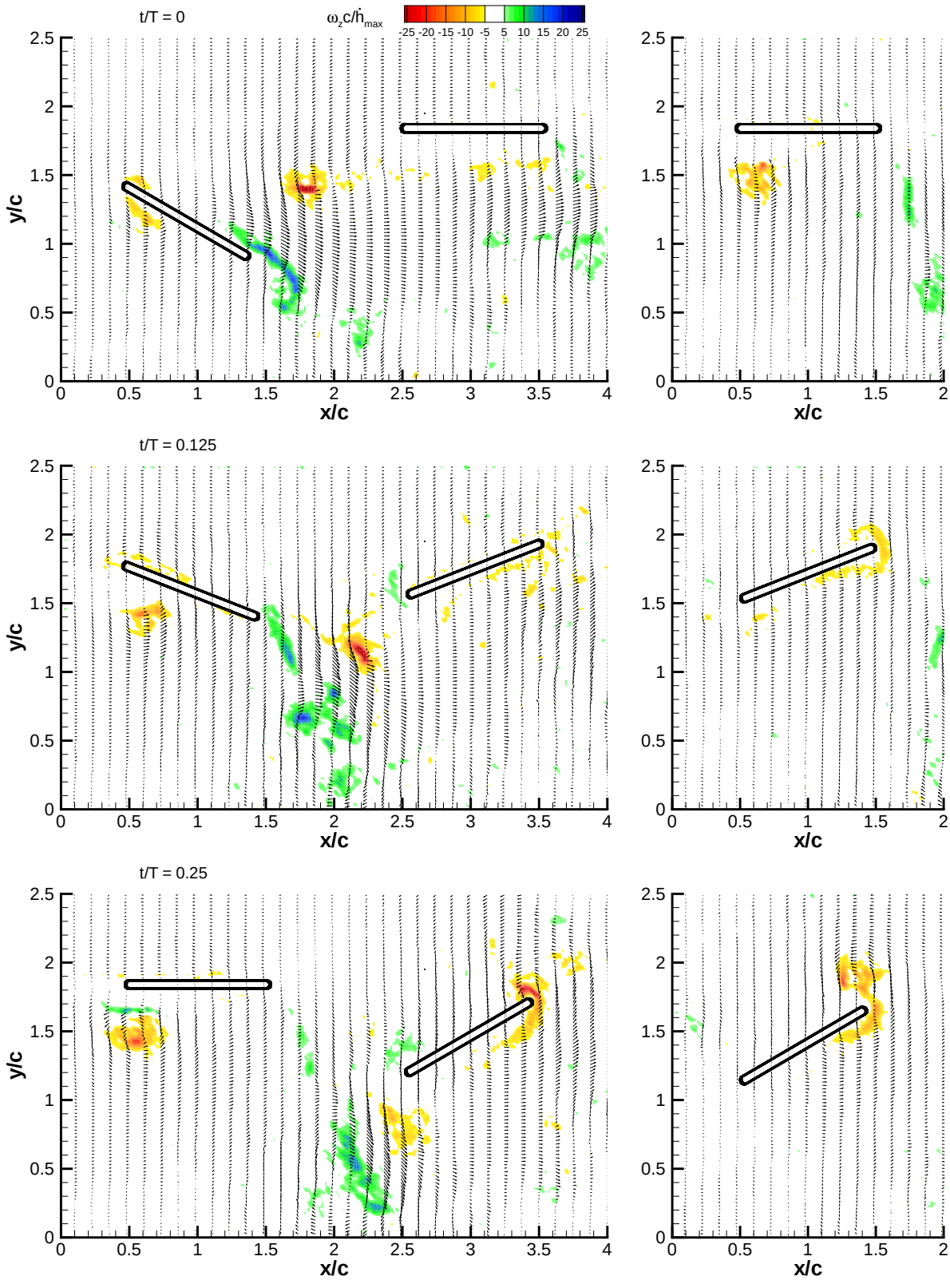

Figure 10.11: Tandem configuration with $\psi = 90°$ (left) and single airfoil (right) during downstroke; note time referenced to hindfoil position for tandem case.

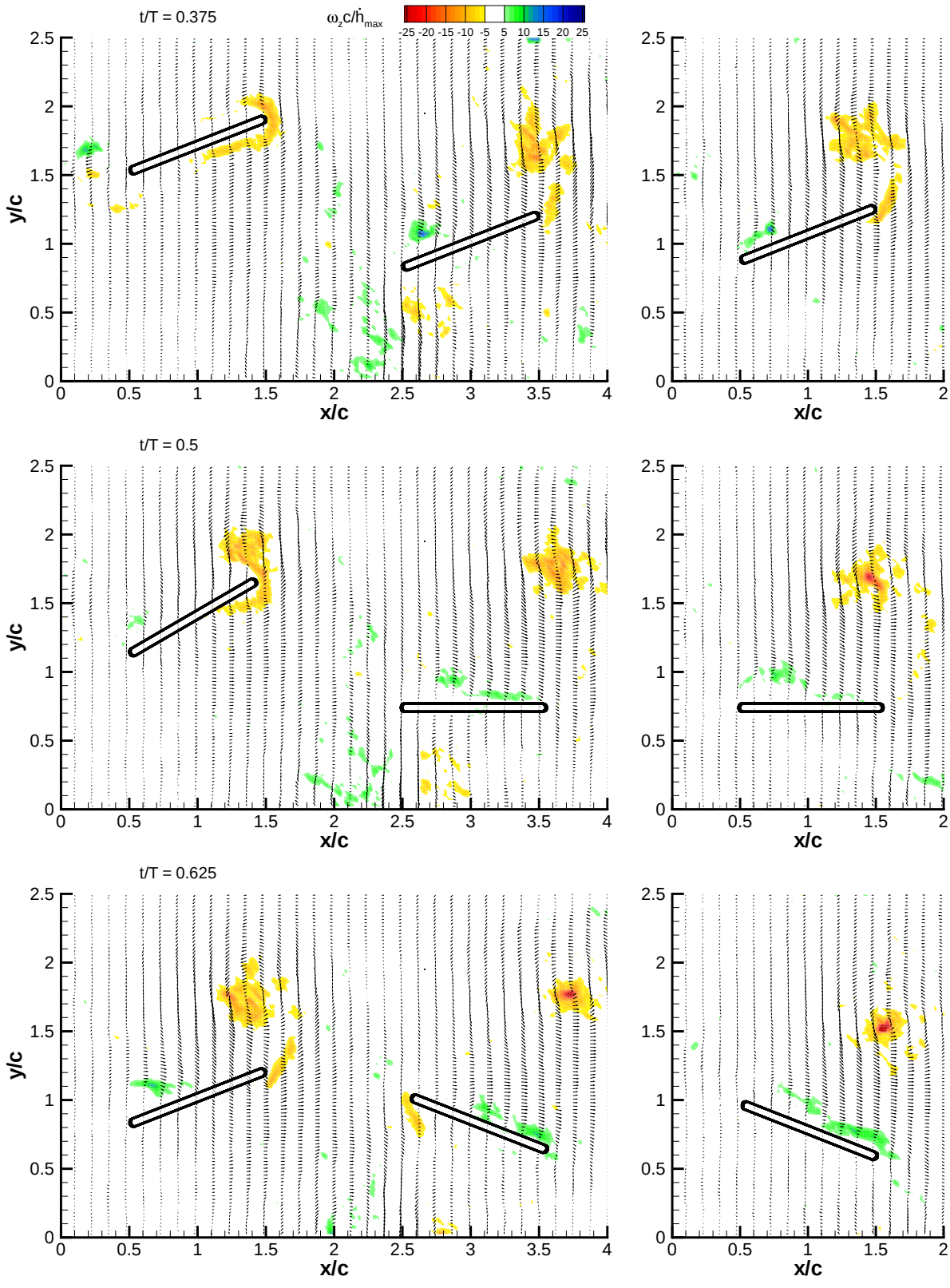

Figure 10.12: Tandem configuration with $\psi = 90°$ (left) and single airfoil (right) around bottom dead center; note time referenced to hindfoil position for tandem case.

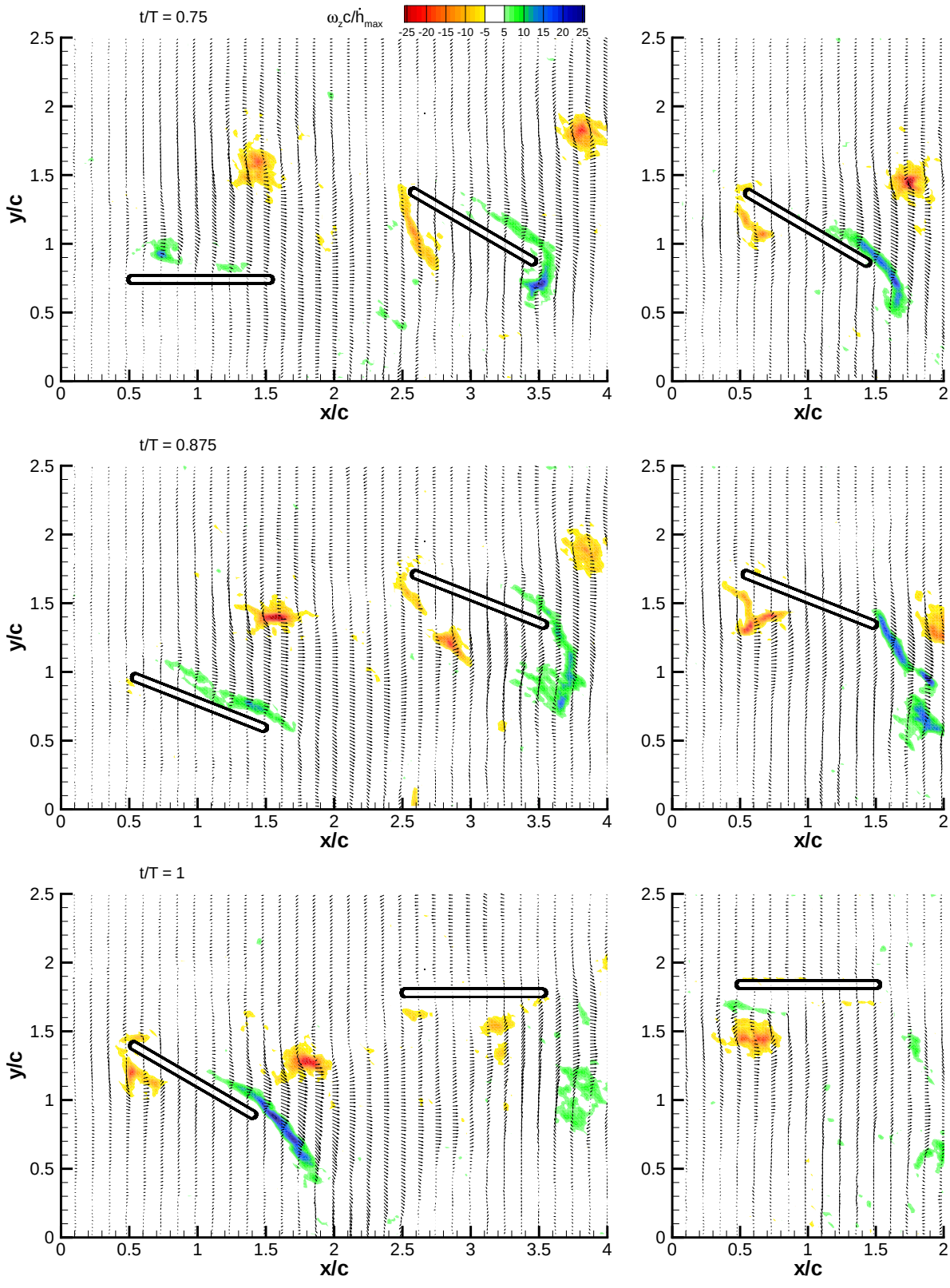

Figure 10.13: Tandem configuration with $\psi = 90°$ (left) and single airfoil (right) during upstroke; note time referenced to hindfoil position for tandem case.

10.6 Summary

In this set of experiments, the influence of phasing on the interaction of two profiles in hover has been investigated. For a phasing of $\psi = 90°$, levels of thrust and power consumption are similar to that of two independent single airfoils. All other phasings shower a drop in performance. The constructive interaction of the forefoil TEV with the hindfoil LEV is responsible for influencing the strength and positing of the hindfoil TEV through mutual induction. In turn the hindfoil TEV is responsible for the timing and strength of the thrust producing jet in the wake. Normal forces and hence power consumption are also varied due to the influence on the hindfoil LEV and TEV production. These results are in good agreement with the three-dimensional flapping experiments of Maybury and Lehmann (2004) and Lehmann (2009), suggesting that the dominant aerodynamic mechanism for hovering in tandem-airfoil configurations is two-dimensional. Thus modifications to the formation of the hindfoil LEV and TEV through either non-sinusoidal kinematics (chapter 6) or three-dimensional, span-wise stabilization (see Ellington (2006) should both result in further improvements in thrust generation and power reduction for such tandem configurations.